Decline of fog, mist and haze in Europe over the past 30 years

Robert Vautard[1]*, Pascal Yiou[1] and Geert Jan van Oldenborgh[2]

Surface solar radiation has undergone decadal variations since the middle of the twentieth century, producing global 'dimming' and 'brightening' effects[1,2]. These variations presumably result from changes in aerosol burden and clouds[3], but the detailed processes involved have yet to be determined. Over Europe, the marked solar radiation increase since the 1980s is thought to have contributed to the observed large continental warming[4], but this contribution has not been quantified. Here we analyse multidecadal data of horizontal visibility, and find that the frequency of low-visibility conditions such as fog, mist and haze has declined in Europe over the past 30 years, for all seasons and all visibility ranges between distances of 0 and 8 km. This decline is spatially and temporally correlated with trends in sulphur dioxide emissions, suggesting a significant contribution of air-quality improvements. Statistically linking local visibility changes with temperature variations, we estimate that the reduction in low-visibility conditions could have contributed on average to about 10–20% of Europe's recent daytime warming and to about 50% of eastern European warming. Large improvements in air quality and visibility already achieved in Europe over the past decades may mean that future reductions in the frequency of low-visibility events will be limited, possibly leading to less rapid regional warming.

Regional amplification of global warming, as observed in Europe over the past 30 years, is a challenging research issue. Models fail to predict the recent 0.5 °C/decade European warming trend[5]. In summer, amplification over land areas may result from feedbacks between air temperature, soil moisture and clouds[6–9]. Large warming trends have also been found in winter or autumn[4,10], associated to a certain extent with circulation changes[5,11], but such changes alone could not explain recent extreme temperature anomalies[12,13]. Atmospheric stability changes due to an increasing greenhouse effect have been suggested as a possible amplifier in a simplified model framework[14], but such changes have not yet been shown in observations.

The upward trend in surface solar radiation since the 1980s (refs 1,2,15) (in Europe about $0.6\,\mathrm{W\,m^{-2}\,yr^{-1}}$) is a candidate for additional warming, especially in populated regions[16]. In Europe, decreasing aerosol burden due to emission reductions is a larger contributor than cloud evolution to decreasing optical depths[3]. However cloud changes, due to relative humidity[17] or aerosol changes, are difficult to characterize because of the poor quality of multidecadal surface or satellite-derived observations[18]. Furthermore, radiation and temperature changes induced by clouds depend critically on the altitude, because high clouds warm and low clouds cool the surface[19]. Recent studies found significant trends in high cloud cover[20,21]. Fog frequency trends have been identified

in individual regions of Europe[22], especially in urban areas, but no synthetic picture has been given so far. In general, the type of cloud and aerosol, and whether they are due to global or regional boundary-layer processes, has not yet been determined.

The analysis of surface horizontal-visibility (v) series provides an ideal framework for this investigation. Phenomena inducing low visibility are either fog ($v \leqslant 1\,\mathrm{km}$), mist ($v \leqslant 2\,\mathrm{km}$) or haze ($v \leqslant 5\,\mathrm{km}$). Data from 342 meteorological stations across Europe are used here. For comparison, the evolutions of collocated cloudiness trends are also carried out. Observations are provided four times daily at 03, 09, 15 and 21 UT. Data and quality control are described in the Methods section.

On average over the selected stations, a strong general decline in the frequency of low-visibility phenomena is found over the past three decades (Fig. 1). For visibilities lower than 2 km, the trend is $-0.3\,\mathrm{day\,yr^{-1}}$ in autumn–winter (Jan.–March and Oct.–Dec.) and -0.1 in spring–summer (April–Sept.), both a 50% reduction over 30 years. The trend is larger for higher thresholds, with $-0.8\,\mathrm{day\,yr^{-1}}$ in autumn–winter (-0.6 in spring–summer) for 5 km visibility, a reduction by more than 50%. A maximal absolute trend is obtained for visibility lower than 8 km, $-1.1\,\mathrm{day\,yr^{-1}}$ in autumn–winter ($-1.2\,\mathrm{day\,yr^{-1}}$ in spring–summer). The values where a decreasing trend is found cover all low-visibility ranges,
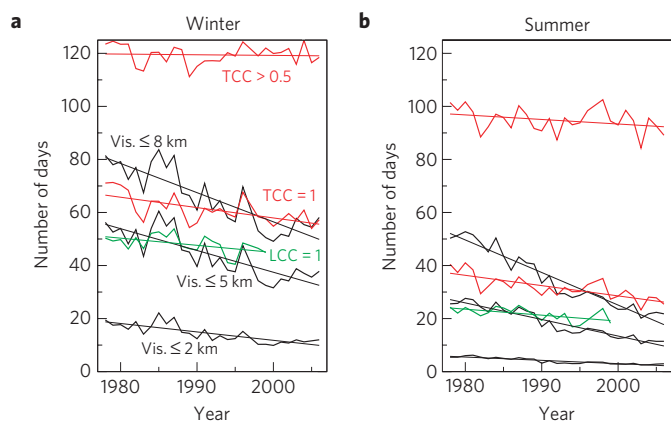

Figure 1 | Time evolution of the number of low-visibility days. a, Time evolution of the mean number of low-visibility and overcast (total cloud cover = 1) weather days in the autumn–winter season (Jan.-March and Oct.-Dec. of each year). For each site and each time (03 UT; 09 UT; 15 UT and 21 UT), the evolution of the number of days per season is calculated. An average over sites and times is then calculated. **b**, The same as **a** for the spring–summer period (April–Oct.). 'Vis' means visibility, 'TCC' means 'total cloud cover' and 'LCC' means 'low cloud cover'.

[1]LSCE/IPSL, laboratoire CEA/CNRS/UVSQ, 91191 Gif sur Yvette Cedex, France, [2]KNMI, PO Box 201, 3730 AE De Bilt, The Netherlands.
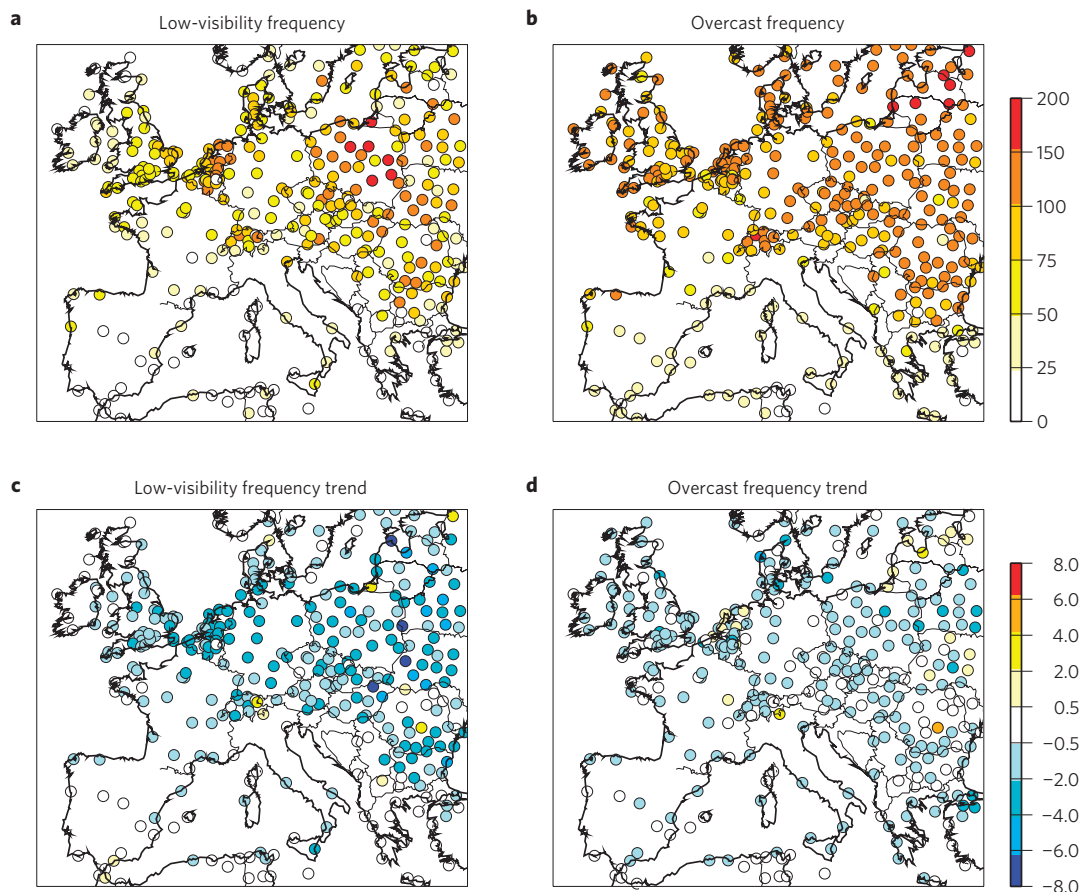*e-mail: robert.vautard@cea.fr.

Figure 2 | Frequency of the low-visibility days and its trend. a,b, Spatial distribution of the annual number of low-visibility days (**a**; $v \leqslant 5$ km) or number of overcast days (**b**), each bullet representing a station used in this study. **c,d,** Trend (in day yr^{-1}) of the number of low-visibility (**c**) or overcast (**d**) days.

including ranges usually associated with low stratus clouds (0–2 km) and dry haze (2–5 km). The decline in low visibility is present for both daytime and night-time hours (not shown). It is also found when restricting the analysis to only clear-sky cases, suggesting a link with the decrease of aerosol burden rather than with cloud changes. The number of overcast observations (sky totally covered) also has a significant, albeit weaker, trend in relative values over Europe, which seems independent of visibility as it is also found when restricting the analysis to high visibilities.

On average low-visibility phenomena (visibility less than 5 km) are found everywhere in Europe, with a much larger frequency in northern Europe (Fig. 2), a behaviour also observed for the frequency of overcast cases. Over southern Europe trends are weaker, owing to the low number of low-visibility cases. Marked trends are present in eastern Europe, consistent with the decline of aerosol loads[23], especially during and after the decline of socialist economies in the late 1980s and early 1990s (see the series at Potsdam station, Supplementary Information, Fig. S1).

A few longer available visibility time series have been analysed (Supplementary Information, Fig. S1), showing in general a decrease in visibilities followed by an increase, with trend reversal times depending on location. In eastern Europe reversal occurs in the 1980s, later than in western Europe (compare series in Supplementary Information, Fig. S1). This peak in low visibility agrees well with the peak in sulphur dioxide emissions in the countries[24], as well as with detailed regional trends in daily temperature range[25]. Moreover, the spatial distribution of 1990–2000 decreases in the frequency of low visibility is significantly correlated with the decrease of sulphur dioxide emission (Fig. 3; $r = 0.56$; $p = 0.01$; rank $r = 0.74$; $p = 3 \times 10^{-6}$),
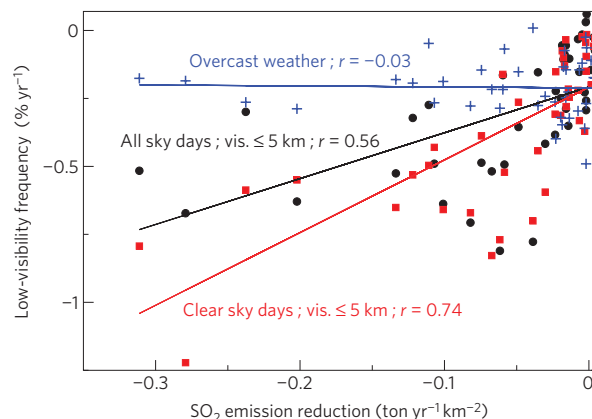

Figure 3 | Low-visibility frequency trend and SO$_2$ emission reductions. Scatter plot of the low-visibility (black circles) and overcast (blue crosses) observation frequency trend versus yearly SO$_2$ emission difference between 1990 and 2000. Both station observations and gridded emissions, coming from the EMEP database[24], are averaged in cells of $5° \times 5°$ size. Red squares stand for the frequency of low-visibility observations among cloud-free observations.

as given by a state-of-the-art inventory[26]. This correlation is enhanced when considering only all-year clear-sky visibility cases (Fig. 3; $r = 0.74$; $p = 2 \times 10^{-4}$; rank $r = 0.80$; $p = 3 \times 10^{-7}$). By contrast, no such correlation is found between SO$_2$ emission reductions and overcast-day frequencies, even though the spatial distributions of overcast and low-visibility observations are similar.
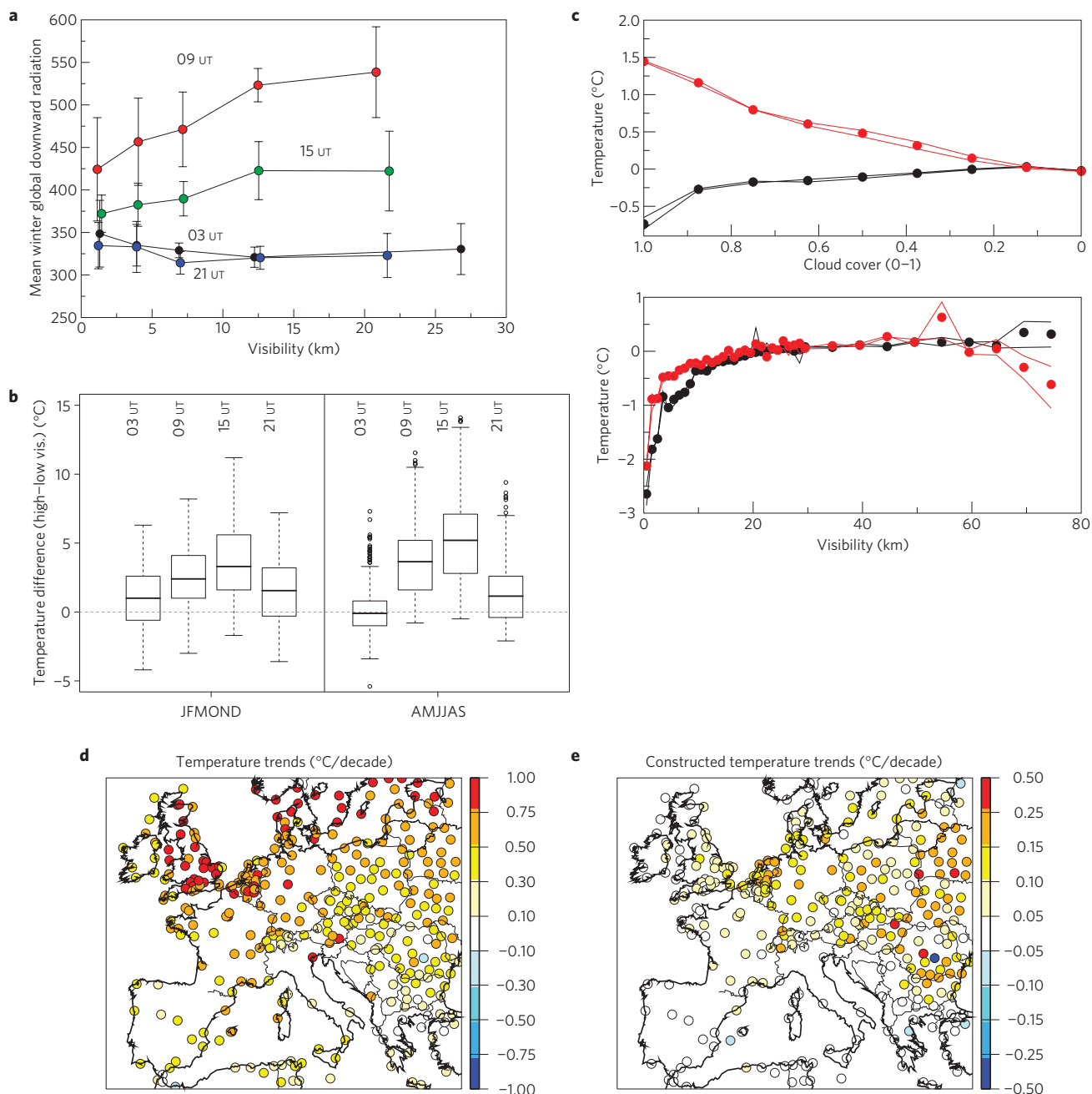
Figure 4 | Low-visibility radiation and temperature. a, Total downward radiation versus visibility during autumn–winter, for four times of the day. Circles stand for averages over visibility bins of 0–2, 2–5, 5–8, 8–15 and 15–100 km. **b**, Temperature difference between high ($v \geq 15$ km) and low ($v \leq 5$ km) visibility, averaged over all sites, for each time. Box-and-whisker plots indicate the 25th, median and 75th quantiles. Lower and upper whiskers denote $\pm 1.5 \times (q_{75} - q_{25}) + q_{50}$. **c**, Sensitivity of local temperature to visibility and cloud cover (see the Methods section). Red (black) curves stand for 03 UT (15 UT). Lines represent values obtained over the first and second halves of the data. **d**, Distribution of total temperature trend in autumn–winter at 15 UT, calculated over 1978–2006. **e**, Constructed temperature trend at 15 UT and for autumn–winter, estimated from the visibility trend and temperature sensitivity.

These results strongly suggest that the air quality improvement during the past decades made a large contribution to the increasing visibility trend.

Low-visibility phenomena alter the surface energy budget by modifying radiation. At a site near Paris[27], changes in visibility from foggy to clear conditions have resulted in significant average changes of 100 W m^{-2} in total (short- and long-wave) downward radiation (Fig. 4a) in autumn–winter during daytime, whereas changes are weak during night time. By enabling less energy to be received at the surface during daytime, the low-visibility phenomenon inhibits surface heating, and therefore induces a lower local temperature. This relative cooling can feed back into radiation by lowering the temperature below the dew point and enabling dense low clouds to form.

Lower temperatures are associated with lower visibilities, as shown in Fig. 4b by the mean temperature difference between high- and low-visibility cases. The much larger daytime than night-time mean temperature difference between low- and high-visibility cases indicates that low-visibility phenomena induce effective temperature changes through radiation as suggested

above. This mechanism is also consistent with the larger daytime than night-time temperature trends[25] (see also Supplementary Information, Table S1).

Assuming now a full causal link between low visibility and temperature, we estimate the sensitivity of local temperature changes to visibility changes for each time and season by linking simultaneous temperature differences with visibility differences in pairs of neighbour sites (Fig. 4c); see the Methods section for details. For comparison the temperature sensitivity to total cloudiness is also calculated.

On average at 15 UT temperatures are about 2 °C lower for low-visibility (less than 2 km) than for high-visibility (more than 15 km) cases in pairs of nearby stations at distances of less than 100 km. The same sensitivity is found at 09 UT as for 15 UT. During the night low visibility remains associated with lower temperatures, in spite of slightly negative total radiation sensitivity (Fig. 4a). Such is not the case for cloud cover: cloudiness leads to a temperature decrease during the day and a temperature increase during the night, with comparable absolute amplitude as for visibility. This indicates a very different night-time sensitivity of temperature to low-visibility phenomena and clouds.

A causal influence of low-visibility phenomena on local temperature should induce a long-term warming. We estimated this trend by multiplying the sensitivity function by the trend of frequency of each visibility bin (see Fig. 4e, Methods section and Supplementary Information, Table S1 for details). This methodology provides a mean induced 0.08 °C/decade daytime temperature trend in autumn–winter, which is about 15–20% of the total trend. Reconstructed daytime warming trends up to 0.2–0.3 °C/decade are found in central and eastern Europe temperatures, which is about 50% of the actual trend (compare Fig. 4d,e). By contrast the induced relative warming is weaker in Mediterranean, western and northwestern and coastal areas. In Mediterranean areas, this results from weak low-visibility frequency trends, whereas in Atlantic areas the warming trend could result from a much higher contribution from sea-surface temperature trends and changes in atmospheric circulation and weather regimes[5]. In summer, daytime visibility trends also potentially induce a warming trend in central and eastern Europe, but the relative contribution is lower because other amplifier processes may dominate, such as coupling with the soil[8]. During the night the local link between visibility and temperature changes is about half as strong as during the daytime. For autumn–winter, the range of visibilities contributing to these estimated trends is essentially 0–5 km (see Supplementary Information, Table S1), fog ($v \leqslant 1$ km) explaining about 20%, mist ($v \leqslant 2$ km) about 50%, and haze ($v \leqslant 5$ km) about 100%. By contrast with visibility, potential effects of cloud-cover trend are small, mean daytime values reaching about 0.02–0.03 °C/decade (only in summer) in absolute values and 4% in terms of relative contribution.

The statistical method to estimate the contribution of low-visibility phenomena to European warming uses several parameters that are taken arbitrarily, such as the maximal distance or altitude difference between site pairs used to calculate the sensitivity functions or the binning of visibility. We have verified that the results are not sensitive to these parameters. In particular, the sensitivity functions can be faithfully reproduced when considering only the first or second half of the data period.

Our approach remains of statistical nature, and the conclusion that daytime temperature trends are potentially influenced by low-visibility phenomenon trends relies on the assumption of a causal relationship through radiation processes. We have shown several results that are consistent with this assumption, but a quantitative understanding of the processes involved requires a regional modelling approach. Unfortunately, current regional climate models are probably not ready to reproduce the physics underlying these trends, because a fully integrated representation of the atmosphere, with surface processes, microphysics coupled with aerosols and gas-phase chemistry models, with relatively high resolution, is required. Also required are databases of the long-term evolution of land use, anthropogenic heat fluxes, aerosol anthropogenic and natural gas species and aerosol emissions. As yet, state-of-the-art regional aerosol models have been shown not to be able to simulate with sufficient skill the total aerosol burden over Europe[28,29]. Simulating trends in low-visibility phenomena, and their impact on climate, therefore remains an open challenge for models.

The major result in this article is the observation of a massive decline (about 50% in 30 years) of low-visibility occurrence throughout Europe. Although at individual sites changes in observing practices may have contributed to the trends, the Europe-wide signal indicates that the trend represents a real change.

The decline of low-visibility phenomena has slowed down since about 2000, as shown in Fig. 1. Although more time is needed to confirm this, such stabilization is expected in the future because (1) European areas with significant frequency of low visibility are currently much reduced from 20 years ago and (2) air quality has improved in Europe in the past two decades owing to emission control policies, resulting in less hope for further improvements.

Methods

Selection of stations. Horizontal-visibility, temperature and cloud-cover data are taken from the NCEP ADP land surface observations available at the National Centre for Atmospheric Research (NCAR) server http://dss.ucar.edu/datasets/ds464.0. We selected 342 European stations (out of 4479) within [10W–30E; 35N–60N] to ensure that all means and regressions are meaningful and that it is possible to compute frequencies of low or high visibility. Details of station selections and of data quality and acquisition are given in Supplementary Information, Methods.

Some visibility-station data, used for constructing Supplementary Information, Fig. S1, cover more extended periods of time and were provided independently by weather services. Radiation data were obtained from the SIRTA observatory site near Paris; see also http://sirta.ipsl.polytechnique.fr.

Cloud-cover data are expressed in octa (0–8). We normalized the values by 8. For cloudy cases, total cloud cover (TCC) or low cloud cover (LCC) is used. TCC = 1 means overcast weather.

Calculation of the sensitivity of temperature to low-visibility phenomena. We investigate the relation between visibility and temperature by computing the mean temperature difference for each station, season and time between high-visibility cases ($v \geqslant 15$ km) and low-visibility cases ($v \leqslant 5$ km). Such temperature differences, shown in Fig. 4b, may be due not to low-visibility phenomena, but to synoptic large-scale weather driving both phenomena. Our procedure to remove the influences of large-scale weather first selects pairs of sites (s_1, s_2) distant by less than 100 km from each other and with altitudes different by less than 50 m. Their simultaneous temperatures T_1 and T_2 are compared as functions of their respective visibilities v_1 and v_2. Taking as a reference for comparison cases when s_1 has a high visibility ($v_1 \geqslant 15$ km), the temperature difference $\Delta T_{1,2} = T_2 - T_1$ determines the influence of low visibility at station s_2. Averaging (overbar operator) these temperature differences $\Delta T_{1,2}$ over all pairs and instants for which $v = v_2$ and $v_1 \geqslant 15$ km leads to a mean temperature-sensitivity-to-visibility function:

$$S(v) = \overline{\Delta T_{1,2} - M_{1,2}}, \qquad (1)$$

where $M_{1,2}$ is the mean systematic temperature difference between pairs of stations. This subtraction removes local land-use or topographic effects. The sensitivity is calculated separately for each time (03, 09, 15 or 21 UT) and each 'season' (autumn–winter, Jan.–March and Oct.–Dec., and spring–summer, April–Sept.).

The constructed trend D due to low-visibility phenomena is calculated by multiplying the sensitivity function $S(v)$ by the visibility frequency trend $D(v)$ in 1 km visibility bins (averaging both sensitivity and visibility frequency between 0–1 km, 1–2 km etc), for each station, season and time:

$$D = \sum_{v=1}^{100\ \text{km}} S(v)D(v). \qquad (2)$$

The visibility frequency trend $D(v)$ is calculated by a linear fit of the time series of seasonal frequencies. Only intervals of v where the trend $D(v)$ can be calculated over more than 10 seasons are considered in equation (2).

For cloud-cover constructed trends the sum in equation (2) is replaced by a sum over the nine values of cloud cover (0–8).

References

1. Wild, M. *et al.* From dimming to brightening: Decadal changes in solar radiation at earth's surface. *Science* **308**, 847–850 (2005).
2. Norris, J. R. & Wild, M. Trends in aerosol radiative effects over Europe inferred from observed cloud cover, solar dimming, and solar 'brightening'. *J. Geophys. Res. Atmos.* **112**, doi:10.1029/2006JD007794 (2007).
3. Ruckstuhl, C. *et al.* Aerosol and cloud effects on solar brightening and the recent rapid warming. *Geophys. Res. Lett.* **35**, L12708 (2008).
4. Xoplaki, E. *et al.* European spring and autumn temperature variability and change of extremes over the last half millennium. *Geophys. Res. Lett.* **32**, L15713 (2005).
5. van Oldenborgh, G. J. *et al.* Western Europe is warming much faster than expected. *Clim. Past Discuss.* **4**, 897–928 (2008).
6. Rowntree, P. R. & Bolton, J. A. Simulation of the atmospheric response to soil-moisture anomalies over Europe. *Quat. J. R. Meteorol. Soc.* **109**, 501–526 (1983).
7. Seneviratne, S. I. *et al.* Land–atmosphere coupling and climate change in Europe. *Nature* **443**, 205–209 (2006).
8. Fischer, E. *et al.* Contribution of land–atmosphere coupling to recent European summer heat waves. *Geophys. Res. Lett.* **34**, L06707 (2007).
9. Vautard, R. *et al.* Summertime European heat and drought waves induced by wintertime Mediterranean rainfall deficit. *Geophys. Res. Lett.* **34**, L07711 (2007).
10. Luterbacher, J. *et al.* Exceptional European warmth of autumn 2006 and winter 2007: Historical context, the underlying dynamics, and its phenological impacts. *Geophys. Res. Lett.* **34**, L12704 (2007).
11. Osborn, T. J., Conway, D., Hulme, M., Gregory, J. M. & Jones, P. D. Air flow influences on local climate: Observed and simulated mean relationships for the United Kingdom. *Clim. Res.* **13**, 173–191 (1999).
12. Van Oldenborgh, J. G. How unusual was autumn 2006 in Europe? *Clim. Past* **3**, 659–668 (2007).
13. Yiou, P., Vautard, R., Naveau, P. & Cassou, C. Inconsistency between atmospheric dynamics and temperatures during the exceptional 2006/2007 fall/winter and recent warming in Europe. *Geophys. Res. Lett.* **34**, L21808 (2007).
14. Walters, J. T., McNider, R. T., Shi, X., Norris, W. B. & Christy, J. R. Positive surface temperature feedback in the stable nocturnal boundary layer. *Geophys. Res. Lett.* **34**, L12709 (2007).
15. Sanchez-Lorenzo, A., Brunetti, M., Calbo, J. & Martin-Vide, J. Recent spatial and temporal variability and trends of sunshine duration over the Iberian Peninsula from a homogenized data set. *J. Geophys. Res. Atmos.* **112**, doi:10.1029/2007JD008677 (2007).
16. Alpert, P., Kishcha, P., Kaufman, Y. J. & Schwarzbard, R. Global dimming or local dimming? Effect of urbanization on sunlight availability. *Geophys. Res. Lett.* **32**, L17802 (2005).
17. Dai, A. G. Recent climatology, variability, and trends in global surface humidity. *J. Clim.* **19**, 3589–3606 (2006).
18. Norris, J. R. What can cloud observations tell us about climate variability? *Space Sci. Rev.* **94**, 375–380 (2000).
19. Solomon, S. *et al. Climate Change 2007 : The Physical Science Basis : Contribution of Working Group I to the Fourth Assessment Report of the Intergovernmental Panel on Climate Change* viii, 996 (Cambridge Univ. Press, 2007).
20. Norris, J. R. Multidecadal changes in near-global cloud cover and estimated cloud cover radiative forcing. *J. Geophys. Res. Atmos.* **110**, D08206 (2005).
21. Wylie, D., Jackson, D. L., Menzel, W. P. & Bates, J. J. Trends in global cloud cover in two decades of HIRS observations. *J. Clim.* **18**, 3021–3031 (2005).
22. Sachweh, M. & Koepke, P. Radiation fog and urban climate. *Geophys. Res. Lett.* **22**, 1073–1076 (1995).
23. Krüger, O. & Grassl, H. The indirect aerosol effect over Europe. *Geophys. Res. Lett.* **29**, 1925 (2002).
24. Streets, D. G., Wu, Y. & Chin, M. Two-decadal aerosol trends as a likely explanation of the global dimming/brightening transition. *Geophys. Res. Lett.* **33**, L15806 (2006).
25. Makowski, K., Wild, M. & Ohmura, A. Diurnal temperature range over Europe between 1950 and 2005. *Atmos. Chem. Phys. Discuss.* **8**, 7051–7084 (2008).
26. Vestreng, V. EMEP/MSC-W Technical Report 1/2006 ISSN 1504-6179 (2006).
27. Haeffelin, M. *et al.* A ground-based atmospheric observatory for cloud and aerosol research. *Ann. Geophys.* **23**, 253–275 (2005).
28. Vautard, R. *et al.* Evaluation and intercomparison of ozone and PM10 simulations by several chemistry-transport models over 4 European cities within the City-Delta project. *Atmos. Environ.* **41**, 173–188 (2007).
29. Stern, R. *et al.* A model inter-comparison study focusing on episodes with elevated PM10 concentrations. *Atmos. Environ.* **42**, 4567–4588 (2008).

Author contributions

G.J.v.O. first discovered trends in visibility in Dutch data, and initiated the work. R.V. generalised the work over Europe, planned the experiments and analysed most data. P.Y. did all quality control and part of the statistical analysis. All co-authors produced some of the figures and parts of the text.

Additional information

Supplementary Information accompanies this paper on www.nature.com/naturegeoscience. Reprints and permissions information is available online at http://npg.nature.com/reprintsandpermissions. Correspondence and requests for materials should be addressed to R.V.